Electronic Supplementary Information

Dumbbells, chains, and ribbons: anisotropic self-assembly of isotropic nanoparticles

Enrico Lavagna[a], Sebastian Salassi[a], Davide Bochicchio[a], Giulia Rossi[a]

[a] Physics Department, University of Genoa, Via Dodecaneso 33, 16146 Genoa, Italy

Au NP model

All the simulations relied on the standard Martini force field for both NP core and ligands[1,2]. The reference Au NP has a core size of 2 nm and is functionalized by a thiol mixture composed of the hydrophobic 1-octanethiol (OT) and the negatively charged 11-mercapto-1-undecanesulfonate (MUS), with three different MUS:OT ratios: no OT (all MUS), 33% OT (MUS:OT 2:1), 50% OT (MUS:OT 1:1). The NP model, which is custom developed, was already used and characterized in previous works[3–7]. The core of the NP is composed of 144 Au beads and 60 S beads on the surface, acting as anchoring sites for the ligands. The core diameter is ~ 2 nm and the overall diameter is ~ 4 nm. Au-Au and Au-S interactions are modeled with an elastic network. The MUS ligands are represented by three type C_1 beads and one negatively charged terminal bead (type Q_{da}). The OT ligands are represented by two type C_1 beads. We remark that experimental indications suggest that MUS :OT NPs may have a striped arrangement of their ligands on the NP surface, while the substitution of OT with 3,7 dimethyl octane 1-thiol (brOT) leads to NPs with a disordered ligand arrangement[8]. Our CG ligand model lacks the resolution to distinguish between OT and brOT. Here we arrange hydrophilic and hydrophobic ligands randomly on the surface of the nanoparticles. Previous atomistic investigation of the behavior of striped vs. random NPs in water suggest that it does not depend on

the grafting pattern[9]. Topologies and cofigurations of the NPs used in this work are available in this repository: https://bitbucket.org/biomembnp/biomembnp/src/master/MARTINI/AuNPs/

Model limitations for electrostatic interactions

It is worth reminding that the use of a coarse-grained force field, and in particular of Martini in our case, implies a certain degree of approximation for charged molecules. Indeed, electrostatic interactions are treated with a cut-off of 1.1 nm to Coulomb interactions (to avoid expensive algorithms for long-range interactions)[1]

In our system, in principle, the cut-off to electrostatic interactions can reduce NP-NP electrostatic repulsion, causing an underestimation of the barrier that separates the ion-bridged contact state from the hydrophobic-contact dimer. This underestimation is likely to produce a faster hydrophobic dimerization that in the experiments, which has also the positive side effect of allowing the simulations to reach the equilibrium in reasonable computational times. Experimentally, tuning of the barrier to hydrophobic contact could be achieved by employing slightly different amphiphilic ligands, modifying their length or the nature of the charged terminal.

The mechanism of ion-bridging per se can not be an artifact of the electrostatic cut-off, being a short range effect. Indeed, previous studies employing both coarse-grained models and atomistic force fields confirmed the existence of the ion bridged minimum, which is also consistent with experimental observations.[10,11]

In each of the 15 unbiased simulations analyzed, the NPs were solvated in a box with a physiological concentration of salt (150mM NaCl). We verified that, at all the compositions investigated, the presence of salt did not influence the final aggregate topology (Figure S3, S4 and S5), by performing similar simulations with only the Na+ counterions. In these simulations, the NPs aggregated with topologies coherent with those of the original 15 physiologically solvated systems.

Methods

Hydrophobic contacts and ion-bridged bonds operational definition.   To verify that a pair of NPs is in a state of hydrophobic contact, we check that there are at least 5 contacts (distance<0.6 nm) between the C1 beads of the ligands of the two different NPs. If a pair of NPs is not in hydrophobic contact, it can be in the ion-bridged configuration. The latter condition is verified if at least 5 counterions are in contact (distance<0.6 nm) with two MUS charged terminal beads belonging to the two different NPs. This definition was already used in Ref.[10]

Asphericity.   The asphericity is a geometrical parameter defined for a set of points distributed in a 3D space, in our case the beads of the ligand shell, that goes from 0 (perfect sphere) to 1 (line). We compute it from the eigenvalues λ_i of the gyration tensor:

$$\beta = \frac{3}{2}\lambda_1^2 - \frac{1}{2}\left(\lambda_1^2 + \lambda_2^2 + \lambda_3^2\right) = \frac{3}{2}\lambda_1^2 - \frac{R_G^2}{2}$$

where β is the asphericity, λ_1 the largest of the eigenvalues of the gyration tensor and R_G the radius of gyration.

Simulation parameters. We used Gromacs[12] 2018.6 to perform all the simulations used in this work. We used the leapfrog integrator in the NPT ensemble, with a reference temperature of 310 K and pressure of 1.0 bar. Constant temperature and pressure were provided, in production runs, by the velocity rescale[13] and Parrinello-Rahaman[14] algorithms, respectively. In equilibration runs we used the Berendsen[15] barostat algorithm instead of the Parrinello-Rahaman, to better suppress system size oscillations. All simulations were run with a time-step of 20 fs. The electrostatic interactions were treated with a 1.1 nm cut-off[16]. The temperature coupling constant τ_T was set to 1 ps, and the

pressure coupling constant τ_P was set to 12 and 4 respectively for production and equilibration runs. The compressibility of the system was set at $3 \cdot 10^{-4}$ bar^{-1}.

Free energy calculations. All free energy profiles were obtained using the umbrella sampling[17] method coupled with the WHAM algorithm for error estimation, with the native Gromacs implementation[18,19]. The sampling windows were spaced at 0.15 nm, and the pulling force constant was set to 1500 kJ/mol. Bootstrap analysis was performed with 100 bootstrap samples and tolerance set at $1 \cdot 10^{-6}$.
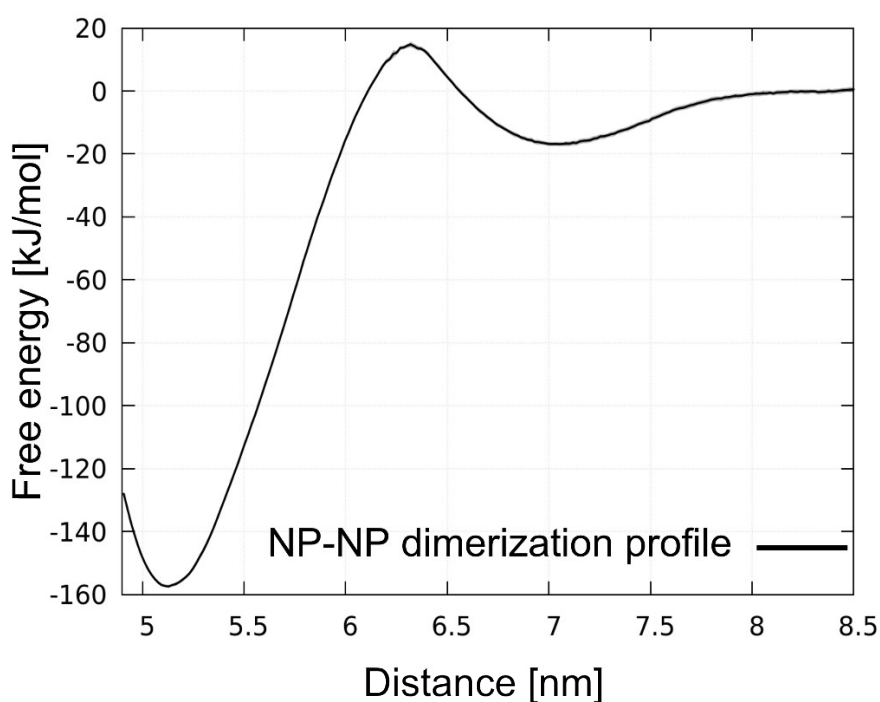

Figure S1: Complete PMF of dimerization PMF of dimerization in water for the MUS:OT 2:1 with a diameter of 4 nm, showing both the ion-bridged minimum (7 nm) and the hydrophobic contact minimum (5.1 nm). Adapted from Ref.[10]

We analyzed the size effect on NP dimerization comparing the results reported in Ref.8 for the 4 nm core model with new simulation with the 2 nm model. Comparing Figure 1c and S1, one can notice that the ion-bridging minimum is more pronounced for the 4 nm NP.

Such a minimum is separated by the lowest-energy hydrophobic contact state by a large barrier (35 kJ/mol).

A simple geometric consideration can explain the difference between the 2 nm and 4 nm profiles. While the core changes size, the ligands remain of the same length and surface grafting density: this implies that the shell of larger NPs will have both a higher packing density and an increased surface charge density. Thus, a concurrent effect of steric confinement and electrostatic repulsion makes interpenetration of the two shells more difficult at larger core sizes.[11]
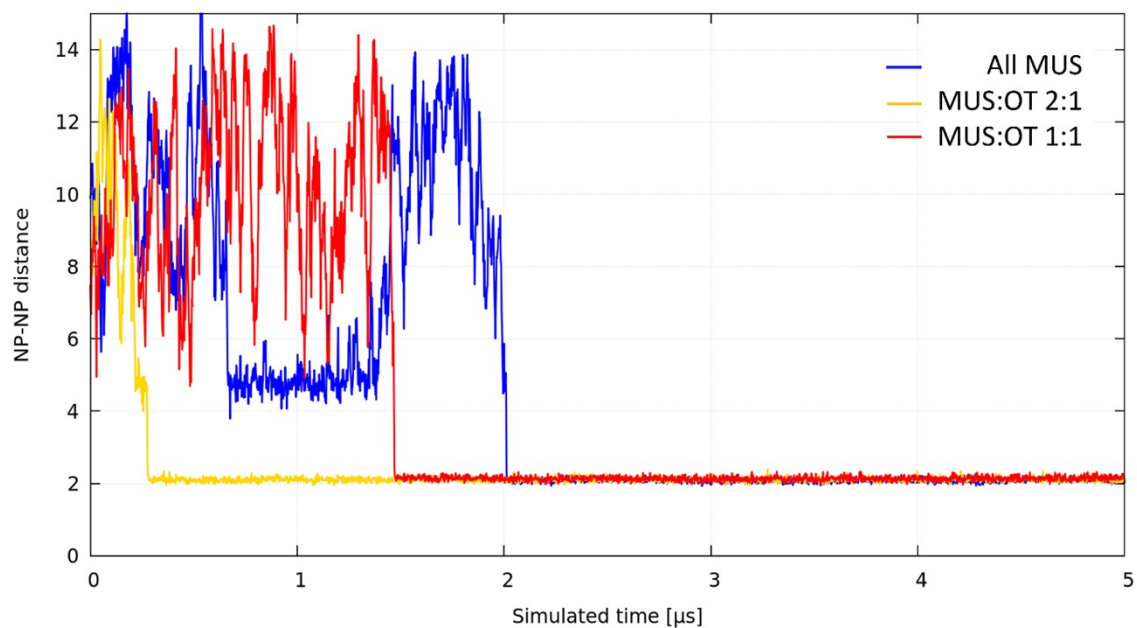
Figure S2: Unbiased dimerization simulation Time evolution of the NP-NP distance in the unbiased dimer simulations at the three different compositions. After 2 μs, the NPs have formed a stable, hydrophobic contact dimer in all three simulations. At around 1 μs, the all MUS NPs form an ion-bridged dimer, which then splits before falling in the hydrophobic contact dimer.
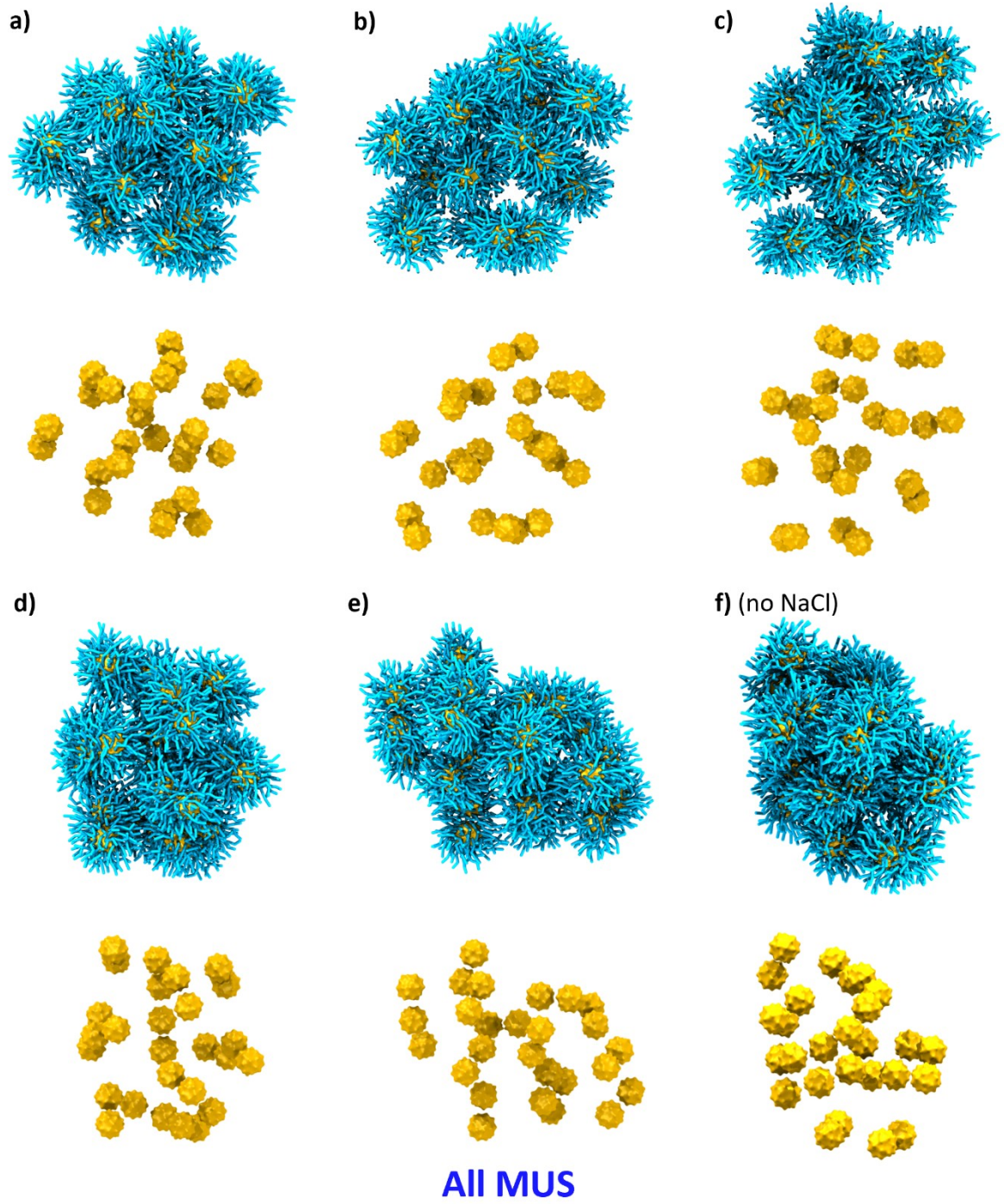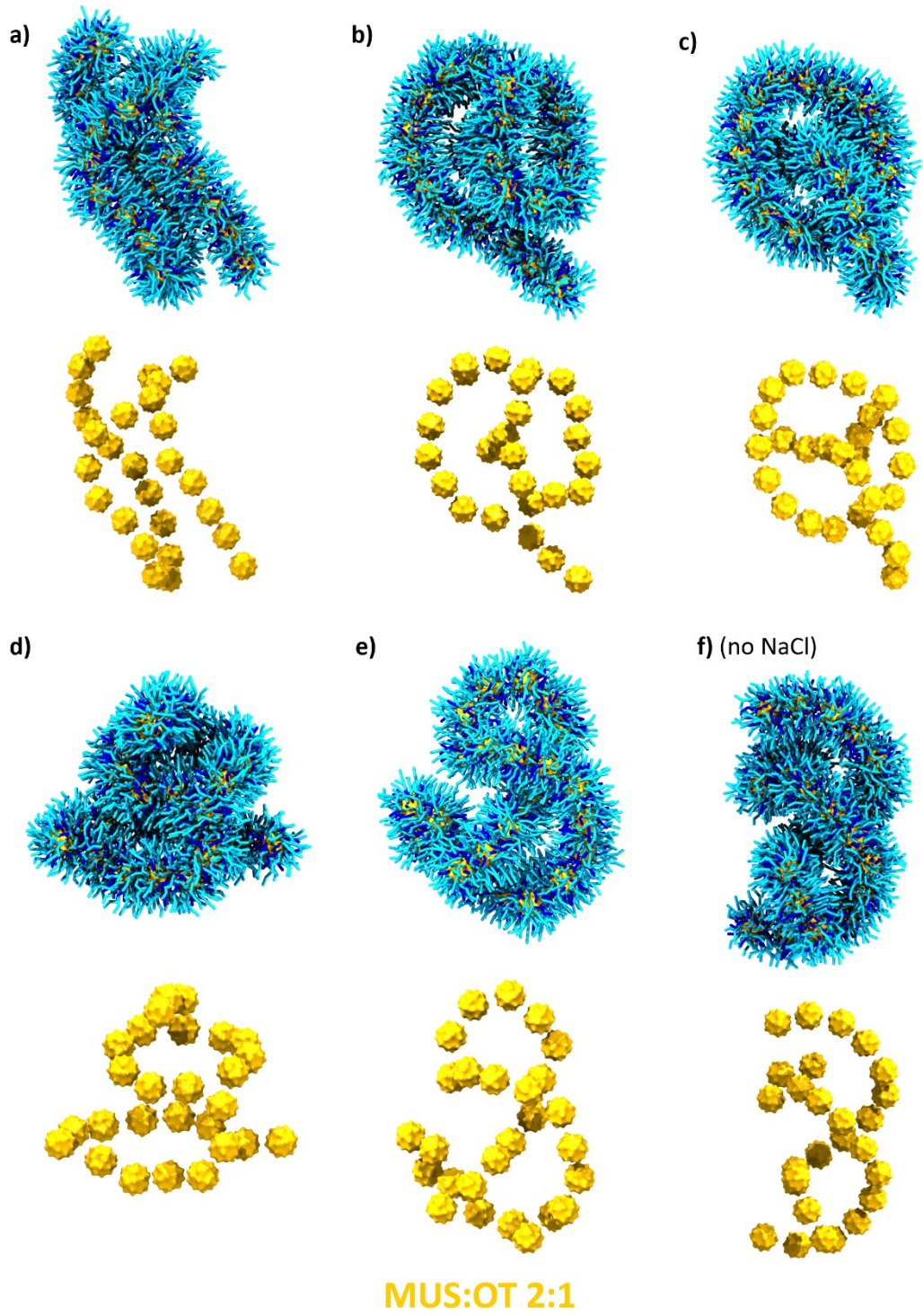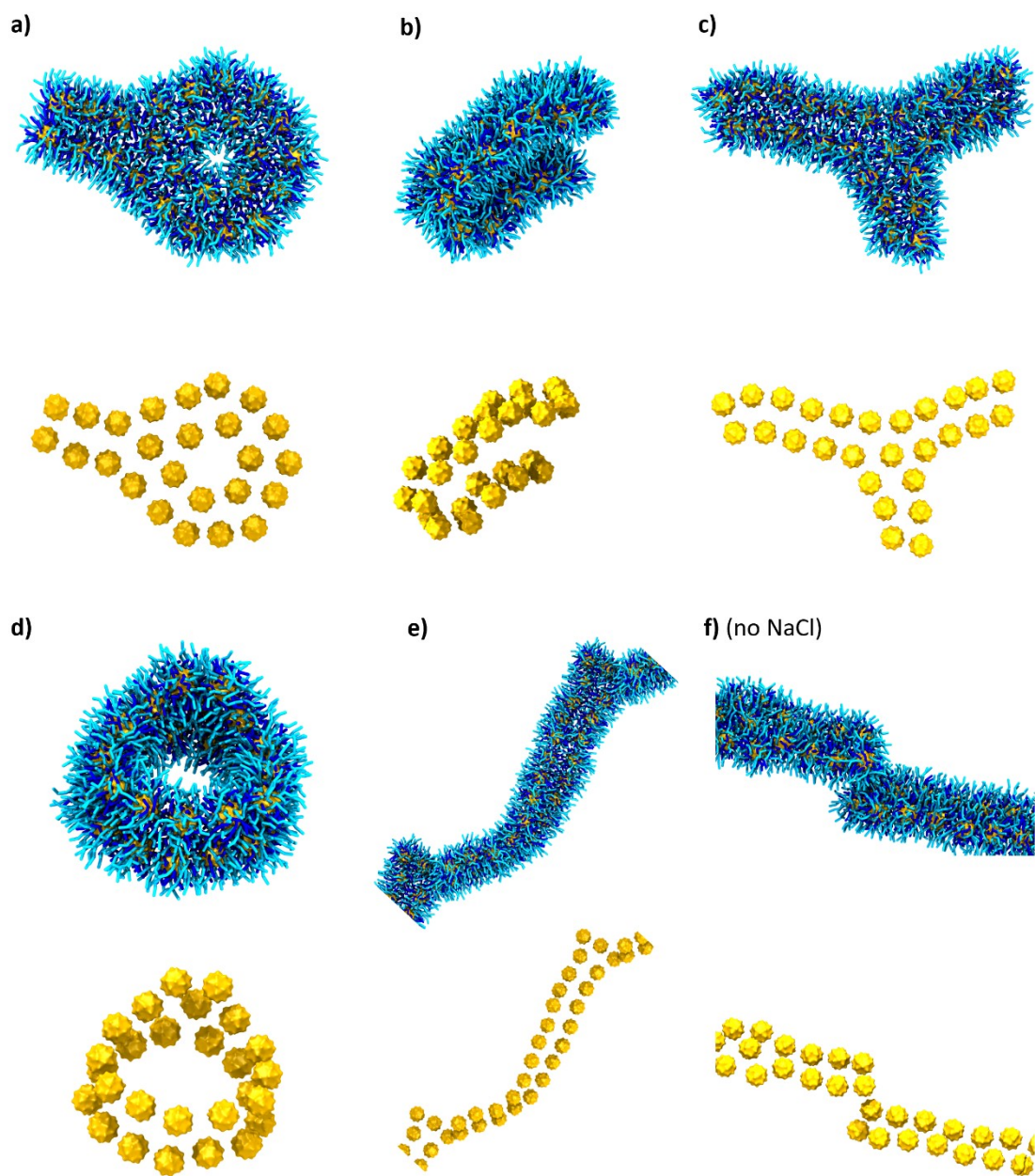
a) b) c)

d) e) f) (no NaCl)

All MUS

Figure S3: All MUS final configurations

MUS:OT 2:1

Figure S4: MUS:OT 2:1 final configurations

a)   b)   c)

d)   e)   f) (no NaCl)

MUS:OT 1:1

Figure S5: MUS:OT 1:1 final configurations
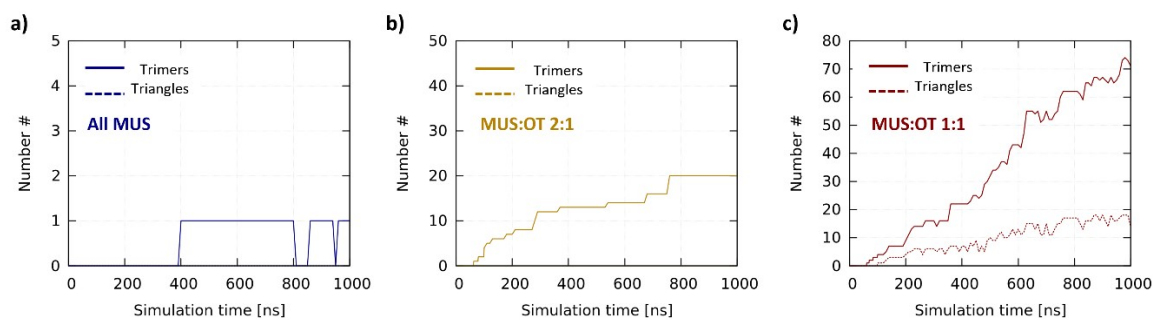
Figure S6: Dynamics of triplet formation. Here, trimers are triplets of NPs connected via 2 hydrophobic bonds, while triangles are triplets in which all the 3 interconnecting bonds are hydrophobic bonds. While all MUS NPs form only one trimer during the aggregate growth, the NPs containing OT form tens of stable trimers. Moreover, the MUS:OT 1:1 NPs also form a significant numbers of triangles.
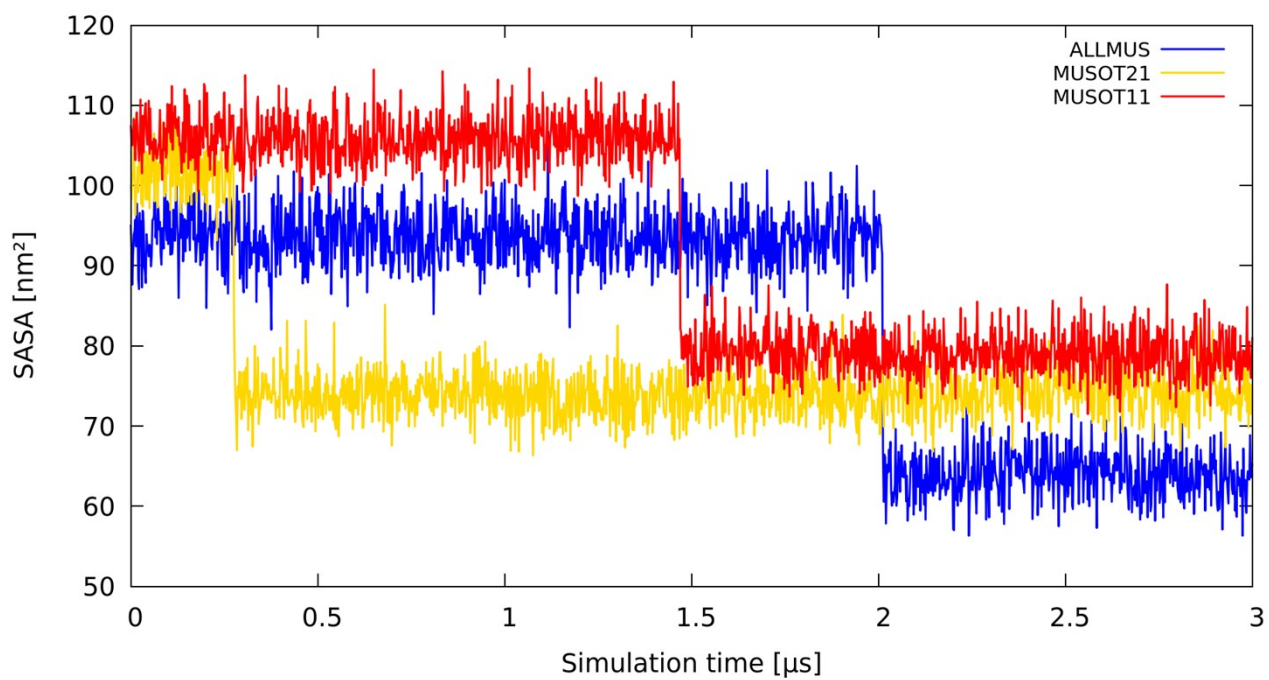
Figure S7: Hydrophobic SASA drop upon dimerization. Time evolution of the overall hydrophobic SASA in the 2 NPs simulations, at the three different compositions. The two time intervals, before and after dimerization, are clearly distinguishable.
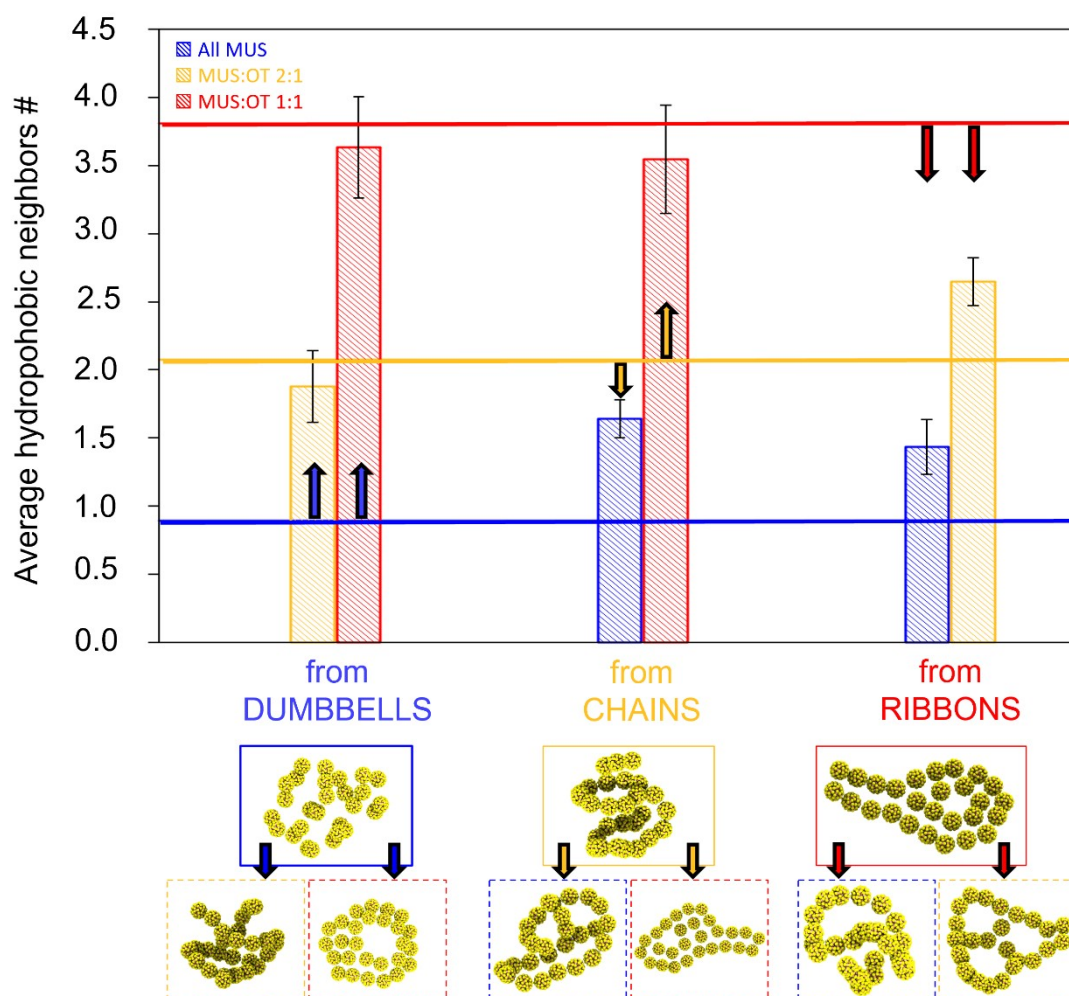
Figure S8: Thermodynamic stability of the native structures In the histogram we show the average number of hydrophobic bonds per NP within the aggregates obtained in the simulations started with a non native aggregate. The histogram's groups are labeled with the topology obtained from the unbiased simulations, which is the starting point for the each of the non-native simulations pairs. The average number of hydrophobic bonds per NP in a certain configuration, as obtained in the unbiased simulation, is represented by a solid line, with color corresponding to the ligand fraction as usual. In the bottom section, we illustrated the starting configurations of the six simulations and the aggregate outcome.

Simulations starting from non-native aggregates

In order to verify that the differences in aggregate topology between NPs of different shell

composition are thermodynamic in nature and not a kinetic effect, we probed the stability of each

topology with each type of NPs. To do this, we recorded the positions of the NP centers of mass in a

certain native aggregate topology (e.g. the cluster of dumbbells obtained with All MUS NPs) and

recreated the aggregate with the two other NP species (e.g. MUS:OT 2:1 and MUS:OT 1:1); we refer

to these configurations as non-native aggregates. The non-native aggregates were initially kept in

place for 1 µs by restraining the positions of the NPs center of mass with a pull potential, in order to allow the ligands to relax. Afterwards, we removed the restraint and ran an unbiased MD for 10 µs. In each case, the topology of the aggregate changes radically in the first few microseconds, as shown in Figure 8. If the OT fraction is higher compared to that of the native NP, new bonds form, as expected. The opposite is also true: if the OT fraction is lower compared to the native NP, the bonds break and the average number of hydrophobic neighbors drops. In the histogram in Figure 8 we show the number of hydrophobic neighbors per NP averaged on the last 3 µs, alongside the same number obtained from the native aggregates (see also Figure 4d). The barrier for breaking is conceivably quite large, which explains the fact that the All MUS NPs do not quite reach the proper topology (cluster of dumbbells) in the simulations starting from non-native topologies. However, the histograms clearly show that NPs of each composition tend to relax towards their number of HC bonds which is typical of their native aggregates, independently from the starting configuration.

1   S. J. Marrink, H. J. Risselada, S. Yefimov, D. P. Tieleman and A. H. de Vries, *J Phys Chem B*, 2007, **111**, 7812–7824.

2   S. J. Marrink and D. P. Tieleman, *Chem Soc Rev*, 2013, **42**, 6801–6822.

3   F. Simonelli, G. Rossi and L. Monticelli, *J Phys Chem B*, 2019, **123**, 1764–1769.

4   F. Simonelli, D. Bochicchio, R. Ferrando and G. Rossi, *Journal of Physical Chemistry Letters*, 2015, **6**, 3175–3179.

5   A. Torchi, F. Simonelli, R. Ferrando and G. Rossi, *ACS Nano*, 2017, **11**, 12553–12561.

6   S. Salassi, F. Simonelli, D. Bochicchio, R. Ferrando and G. Rossi, *Journal of Physical Chemistry C*, 2017, **121**, 10927–10935.

7   S. Salassi, E. Canepa, R. Ferrando and G. Rossi, *RSC Adv*, 2019, **9**, 13992–13997.

8   A. Verma, O. Uzun, Y. Hu, Y. Hu, H. S. Han, N. Watson, S. Chen, D. J. Irvine and F. Stellacci, *Nat Mater*, 2008, **7**, 588–595.

9   R. C. Van Lehn and A. Alexander-Katz, *The Journal of Physical Chemistry C*, 2013, **117**, 20104–20115.

10   E. Lavagna, D. Bochicchio, A. L. De Marco, Z. P. Güven, F. Stellacci and G. Rossi, *Nanoscale*, 2022, **14**, 6912–6921.

11   E. Petretto, Q. K. Ong, F. Olgiati, T. Mao, P. Campomanes, F. Stellacci and S. Vanni, *Nanoscale*, 2022, **14**, 15181–15192.

12   M. J. Abraham, T. Murtola, R. Schulz, S. Páll, J. C. Smith, B. Hess and E. Lindahl, *SoftwareX*, 2015, **1–2**, 19–25.

13   G. Bussi, D. Donadio and M. Parrinello, *J Chem Phys*, 2008, **126**, 014101.

14   M. Parrinello and A. Rahman, *J Appl Phys*, 1981, **52**, 7182–7190.

15   D. H. de Jong, L. v. Schäfer, A. H. de Vries, S. J. Marrink, H. J. C. Berendsen and H. Grubmüller, *J Comput Chem*, 2011, **32**, 1919–1928.

16   D. H. de Jong, S. Baoukina, H. I. Ingólfsson and S. J. Marrink, *Comput Phys Commun*, 2016, **199**, 1–7.

17   G. M. Torrie and J. P. Valleau, *J Comput Phys*, 1977, **23**, 187–199.

18   J. S. Hub, B. L. de Groot and D. van der Spoel, *J Chem Theory Comput*, 2010, **6**, 3713–3720.

19   S. Kumar, J. M. Rosenberg, D. Bouzida, R. H. Swendsen and P. A. Kollman, *J Comput Chem*, 1992, **13**, 1011–1021.